


Article

# Hierarchical ZSM-5 Zeolite with Enhanced Catalytic Activity for Alkylation of Phenol with Tert-Butanol

Ling Xu <sup>1,\*</sup>, Fan Wang <sup>1</sup>, Zhiqiang Feng <sup>1</sup>, Zongrui Liu <sup>1</sup> and Jingqi Guan <sup>2,\*</sup> 

<sup>1</sup> College of Chemistry and Chemical Engineering, Inner Mongolia University for Nationalities, Tongliao 028000, China; wf18848176887@163.com (F.W.); zhiqiangfeng@163.com (Z.F.); liuzr716@163.com (Z.L.)

<sup>2</sup> College of Chemistry, Jilin University, Changchun 130023, China

\* Correspondence: tlxuling1979@163.com (L.X.); guanjq@jlu.edu.cn (J.G.)

Received: 31 December 2018; Accepted: 19 February 2019; Published: 23 February 2019



**Abstract:** Using polyethylene glycol as a mesoporous soft template, a series of hierarchically porous ZSM-5 zeolites were prepared. X-ray diffraction, infrared spectroscopy, N<sub>2</sub> adsorption–desorption, and transmission electron microscopy results demonstrated that the resultant materials contained a micro–mesoporous structure. Since the existence of mesoporous structure favors the diffusion of large molecular reactants and products, the phenol conversion and selectivity to 2,4-Di-TBP on the hierarchical ZSM-5 zeolite can be improved for the alkylation of phenol with tert-butanol.

**Keywords:** ZSM-5 zeolite; micro–mesoporous structure; phenol; tert-butanol; alkylation

## 1. Introduction

Zeolites have been applied widely as catalysts due to their high specific surface area and catalytic acidity, which comes from replacing a little silicon dioxide with aluminum oxide. In the past decades, zeolite ZSM-5 has played a significant role in the chemical industry due to some properties, such as exceptional three-dimensional pore structure without cage construction, acid resistance, thermal stability, and hydrophobic resistance [1–10]. However, the traditional ZSM-5 has only a microporous structure, greatly limiting the applications in the field of catalysis. Therefore, structuring hierarchically porous zeolites ignites great interests in materials science. Compared with microporous molecular sieves, micro–mesoporous molecular sieves provide mesoporous pores that greatly improve the mass transfer ability. Moreover, the acidity and hydrothermal stability of the pore walls are enhanced with partial crystallization, improving acid-catalytic performance [11–18].

There are many methods for synthesizing micro-intermediate composite pore molecular sieves reported previously, mainly including alkaline treatment methods, desilication and dealumination methods, soft and hard template methods, etc. The alkaline treatment dealumination method generally removes aluminum in the molecular sieve skeleton by calcination, hydrothermal treatment, chemical treatment, etc., thereby forming a hole defect mesoporous structure. This method has the disadvantages of poor connectivity of the introduced mesoporous structure, reduction of molecular crystallinity, reduction of the number of acidic centers, and the aluminum fragments formed in the process of dealumination are liable to block the micropore channels. The alkaline treatment desilication method destroys the skeleton silicon in the molecular sieve by alkaline treatment, thereby introducing a mesoporous structure [19]. The method has some advantages, such as low cost and simple operation, and is widely used in industrialization. However, the mesoporous structure formed is irregular, and the skeleton silicon is excessively removed to form a large aperture channel. The hard template method uses carbon nanotubes, activated carbon or the like as a hard template to crystallize the silicoaluminol sol under hydrothermal conditions, and then the templating agent is removed by baking

or the like to form a mesoporous structure [20]. The size of mesoporous structure synthesized by this method is controllable, and the mesoporous channels are uniformly distributed. However, strict control conditions are required in the preparation of mesoporous zeolite, which is not easy to apply to industrialization. The soft template method uses a surfactant, organosilane, water soluble polymer or the like as a template to interact with a silicon–aluminum species in a molecular sieve to form an ordered mesoporous structure. The method has the advantages of simple operation, wide selection of template agent, and adjustable pore size of mesoporous molecular sieve. Guo et al. [21] used organosilane coupling agent as template by high-temperature crystallization to obtain multi-stage pores of ZSM-5 molecular sieve. Liu et al. [22] used a cationic amphiphilic polymer as a template to synthesize a hierarchical pore ZSM-5 molecular sieve, which had excellent catalytic performance for the catalysis of macromolecular compounds. Although the soft template method has the above advantages, the soft template agent has the disadvantages of high cost and environmental pollution.

Herein, we take advantage of inexpensive polyethylene glycol (PEG) as a mesoporous soft template to prepare hierarchically porous zeolite ZSM-5 by means of sol–gel controlling. PEG can transform into ordered and orientated micelle in the existence of sodium ions, which plays a structure-directing role. The prepared micro–mesoporous materials with different conditions were evaluated in the phenol tert-butylation reaction to optimize the synthetic parameter.

## 2. Results and Discussion

### 2.1. Catalytic Performance of Micro–Mesoporous ZSM-5 with Different Stirring Time

The XRD patterns of the samples synthesized under different stirring time are depicted in Figure 1. For the sample with exposed stirring time of 3, 6, and 9 h, the XRD pattern showed that the sample was mainly amorphous. However, MZ-15-3.2 with a stirring time of 15 h showed several diffraction peaks at  $7.9^\circ$ ,  $8.8^\circ$ ,  $23.1^\circ$ ,  $23.9^\circ$ , and  $24.4^\circ$ , corresponding to the characteristic peaks of the MFI (mobile five) topology. Therefore, extending the exposed stirring time is beneficial to the improvement of ZSM-5 crystallinity.

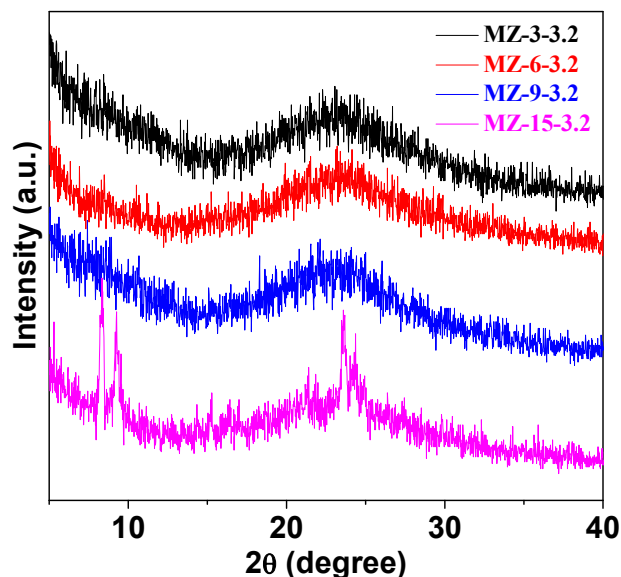


Figure 1. XRD patterns of MZ-3-3.2, MZ-6-3.2, MZ-9-3.2, and MZ-15-3.2.

The Fourier-transform infrared (FT-IR) spectra of ZSM-5 prepared under different exposed stirring time are depicted in Figure 2. All the samples have two distinct absorption bands at ca.  $1228$  and  $800\text{ cm}^{-1}$ , assigned to the antisymmetric stretching vibrations and symmetric stretching vibrations of Si–O–Si, respectively. While with the increasing exposed stirring time, especially for

9 and 15 h, a new band located at  $550\text{ cm}^{-1}$  corresponding to characteristic absorption peaks of ZSM-5 zeolite was distinctly seen, indicative of generating micropore structure. The samples also developed bands at ca.  $3430$  and  $1630\text{ cm}^{-1}$ , which was ascribed to the absorbed water. The band at  $\sim 2900\text{ cm}^{-1}$  was assigned to C–H stretch of the small quantity of residual template. The morphology of MZ-9-3.2 was characterized by HRTEM. As shown in Figure 3, the sample did not show ordered mesoporous structure, indicating that polyethylene glycol acts as a pore former and only generates some irregular mesopore.

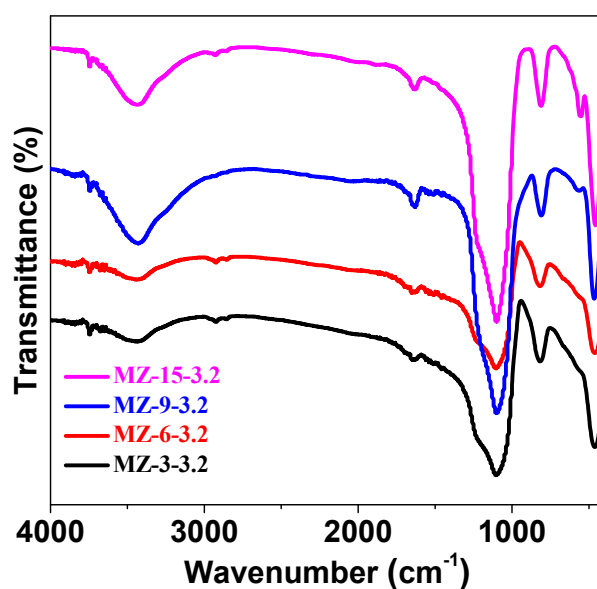


Figure 2. FT-IR spectra of MZ-3-3.2, MZ-6-3.2, MZ-9-3.2, and MZ-15-3.2.

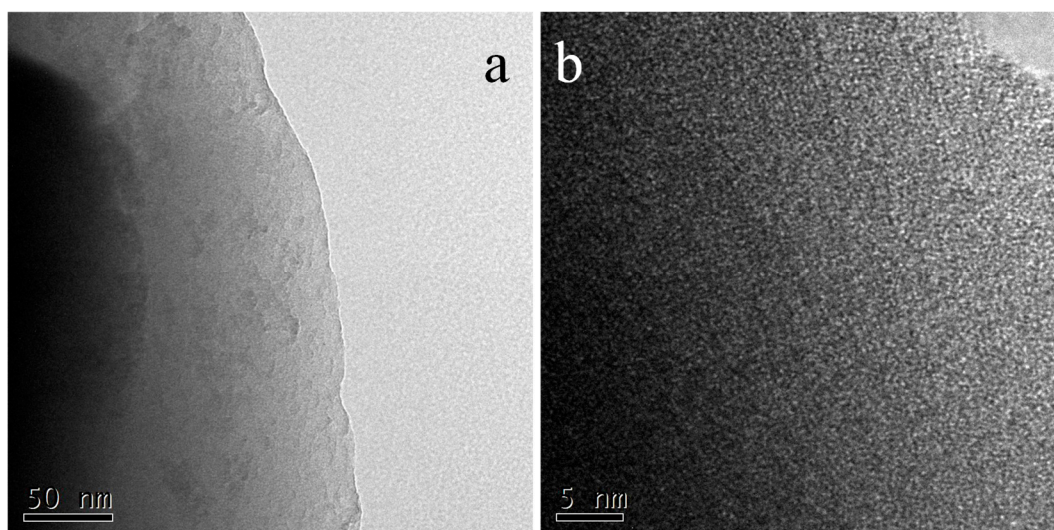
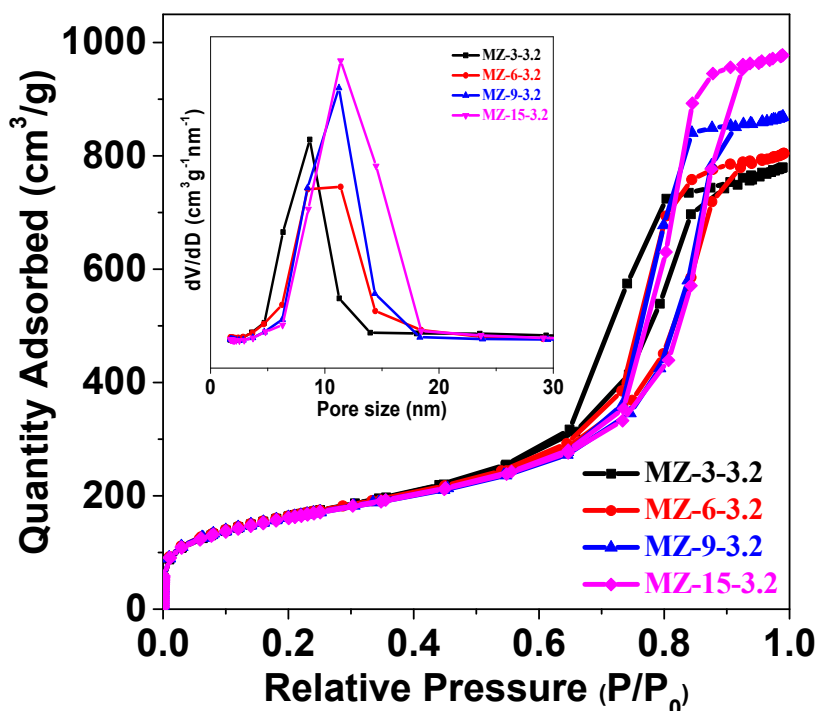


Figure 3. HRTEM images of MZ-9-3.2 with (a) low magnification and (b) high magnification.

The  $\text{N}_2$  adsorption–desorption isotherm curves of the samples are presented in Figure 4. The samples with different exposed stirring time exhibit a type IV adsorption curve accompanied by a significant hysteresis loop, indicating that all the samples contained mesoporous structure, which was attributed to the influence of polyethylene glycol as a mesoporous template in the synthesis process. In addition, as the exposed stirring time was extended, the hysteresis loop of the sample was close to the type  $\text{H}_2$ , indicating that the mesoporous distribution was more regular. The BJH pore size distribution of the sample is depicted in the inset of Figure 4. The BJH pore size of the sample increased with the increase

of the exposed stirring time from 3 to 6 h, which almost remained constant with further increasing the exposed stirring time (Table 1).



**Figure 4.**  $N_2$  adsorption–desorption isotherms of and the BJH pore size distribution of MZ-3-3.2, MZ-6-3.2, MZ-9-3.2, and MZ-15-3.2.

The pore parameters of the samples are listed in Table 1. When the exposed stirring time was extended from 3 to 15 h, the BET specific surface area of the sample slightly decreased from  $592 \text{ m}^2 \cdot \text{g}^{-1}$  to  $579 \text{ m}^2 \cdot \text{g}^{-1}$ . The specific surface area of the micropore gradually increased, indicating that a certain microporous structure was formed.

**Table 1.** Pore parameters of the samples.

Sample	$S_{\text{BET}}$ ( $\text{m}^2 \cdot \text{g}^{-1}$ )	Microporosity			Mesoporosity		
		Area ( $\text{m}^2 \cdot \text{g}^{-1}$ )	Size (nm)	Volume ( $\text{cm}^3 \cdot \text{g}^{-1}$ )	Area ( $\text{m}^2 \cdot \text{g}^{-1}$ )	Size (nm)	Volume ( $\text{cm}^3 \cdot \text{g}^{-1}$ )
MZ-3-3.2	592	39	–	0.01	553	8.6	1.20
MZ-6-3.2	589	64	–	0.02	525	11.1	1.24
MZ-9-3.2	581	75	–	0.03	506	11.3	1.34
MZ-15-3.2	579	158	–	0.02	421	11.3	1.51

Figure 5 shows the  $\text{NH}_3$ -TPD profiles of the samples with different stirring time. Two obvious  $\text{NH}_3$ -desorption peaks were attributed to the desorption of ammonia in the weak acid and strong acid centers. The temperature of the  $\text{NH}_3$ -desorption peak of MZ-3-3.2 and MZ-6-3.2 was relatively low, while the temperature of the  $\text{NH}_3$ -desorption peak of MZ-9-3.2 and MZ-15-3.2 was relatively high, indicating that the longer the stirring time the stronger the acidity formed in the sample.

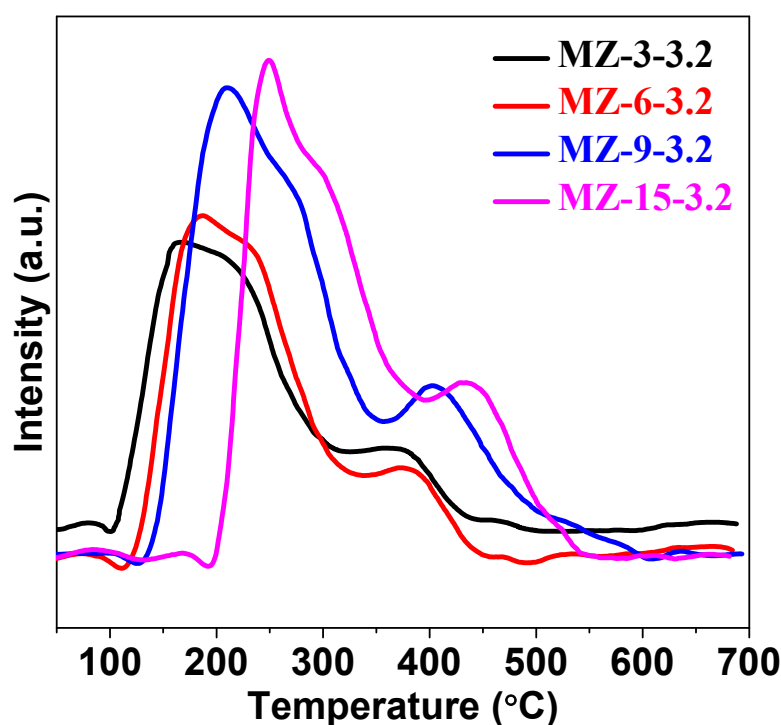


Figure 5.  $\text{NH}_3$ -TPD profiles of MZ-3-3.2, MZ-6-3.2, MZ-9-3.2, and MZ-15-3.2.

The reaction of phenol with tert-butanol is a typical Friedel–Crafts alkylation reaction. The conversion of phenol and the selectivity of the main product 2,4-Di-tert-butylphenol are usually used as a measurement index of catalytic performance. The alkylated product of 2,4-Di-tert-butylphenol (2,4-Di-TBP) is an important intermediate, which is widely applied in industry as raw material for the preparation of a variety of resins, antioxidants, varnishes, surface-active agents, ultraviolet absorbers, petroleum additives, and so on.

It can be seen from Table 2 that the catalytic performance of the sample is improved to a certain extent by extending the exposed stirring time during the synthetic process. When the exposed stirring time was extended to 9 h, the conversion of phenol was highest (reaching 96.5%) and the selectivity to the macromolecular products 2,4-Di-TBP and 2,4,6-Tri-tert-butylphenol (2,4,6-Tri-TBP) was also the best. However, when the exposed stirring time was further extended to 15 h, the conversion of phenol was slightly reduced.

Table 2. The reaction results of the alkylation of phenol with tert-butanol. <sup>a</sup>

Catalyst	Conversion (%)	Selectivity (%)			
		2-TBP	4-TBP	2,4-Di-TBP	2,4,6-Tri-TBP
MZ-3-3.2	83.5	4.7	53.4	41.7	0.2
MZ-6-3.2	84.9	5.4	46.3	48.0	0.3
MZ-9-3.2	96.5	6.2	39.2	53.9	0.7
MZ-15-3.2	92.0	6.2	50.4	42.9	0.4

<sup>a</sup> Reaction temperature: 418 K; Phenol:TBA = 1:2.5 (molar ratio); WHSV = 2.2  $\text{h}^{-1}$ ; TBP: tert-butylphenol.

In addition, MZ-15-3.2 and MZ-9-3.2 showed the same mesopore size and similar mesopore volume, but different mesoporous surface area and very different acid strength. The alkylation reaction mainly occurred on the acidic sites of mesopore surface. Compared with MZ-15-3.2, MZ-9-3.2 showed higher phenol conversion and selectivity to bulky 2,4-Di-TBP mainly due to the larger mesopore surface area and weaker acid strength, as shown in Figure 5. Moreover, MZ-3-3.2 and MZ-6-3.2 had larger mesopore surface areas than MZ-9-3.2 as shown in Table 1. However, the catalytic activity and

selectivity to 2,4-Di-TBP on MZ-3-3.2 and MZ-6-3.2 were lower than those on MZ-9-3.2, which was attributed to the different acidity of catalyst. It is reported that the alkylation of phenol with tert-butanol is an acid-catalyzed reaction and the appropriately strong acidity of the catalyst is beneficial to this reaction. The acidity of MZ-3-3.2 and MZ-6-3.2 was weaker than that of MZ-9-3.2, as shown in Figure 5. Hence, the high conversion and selectivity to 2,4-Di-TBP over MZ-9-3.2 could be assigned to the proper mesopore surface area and acidity.

The comparison of the as-obtained catalyst and some reported catalysts for the alkylation of phenol with tert-butanol is shown in Table 3. As mentioned above, the alkylation of phenol with tert-butanol is an acid-catalyzed reaction. Appropriately strong acidity of microporous zeolite, such as ZSM-5, HY [23,24], and so on, is beneficial to this reaction. However, the small pore size made it very difficult for the large size molecules to diffuse effectively in the pore system. Accordingly, the reaction mainly occurred on the external surface of micropore catalysts, where the amount of acidic sites was relatively small. As a result, the conversion of phenol on conventional ZSM-5 and HY was relatively low. It is worth mentioning that the phenol conversion on microporous zeolite H $\beta$  [25] was higher than that on ZSM-5 and HY, which was mainly attributed to the larger micropore size of H $\beta$ . However, the selectivity to the 2,4-Di-TBP on H $\beta$  was still lower than that achieved on MZ-9-3.2 due to the disadvantage of large molecule mass transfer and diffusion in micropore zeolite. Additionally, Sakthivel et al. [26] reported the alkylation of phenol with tert-butanol over Al-MCM-41 mesoporous molecular sieve. Although Al-MCM-41 has the mesoporous channels, its catalytic activity was still low, which should be ascribed to weak acidity of amorphous mesoporous walls. The differences of catalytic activity between the conventional micropore zeolite, mesopore molecular sieve, and the hierarchical zeolite could be mainly attributed to their different pore structure property and acidity [27,28]. Hence, the proper pore structure and acidity in the hierarchical ZSM-5 zeolite enabled much easier diffusion of reactants and products, favoring a high phenol conversion and high selectivity to 2,4-Di-TBP.

**Table 3.** The compared results of alkylation of phenol with tert-butanol on different catalysts.

Catalysts	$n_{\text{phenol}}/n_{\text{tert-butanol}}$	WHSV (h <sup>-1</sup> )	T (°C)	Phenol Conversion (%)	Selectivity (%)			Ref.
					2-TBP (%)	4-TBP (%)	2,4-Di-TBP (%)	
MZ-9-3.2	0.4	2.20	145	96.5	6.2	39.2	53.9	This work
HY	0.5	2.4	200	28.6	11.7	69.7	14.6	23
HY-550	0.5	2.4	200	62.5	8.5	75.9	9.5	23
H $\beta$	2	0.67	145	96.2	2.99	76.38	20.63	24
ZSM-5	0.4	2.2	145	36.7	16.8	42.6	40.6	25
AlMCM-41(56)	0.5	4.5	175	35.9	8.1	83.4	3.9	26
H-AlMCM-41	0.5	4.8	215	64.1	1.7	29.9	1.4	26
FIBAN K1	3	–	100	23	58	33	10	27
HZ5-A	0.5	–	125	32	10	70	20	28

## 2.2. Catalytic Performance of Micro–Mesoporous ZSM-5 with Different PEG Dosage

The XRD spectra of samples with different PEG dosage are depicted in Figure 6. The sample without dosage of PEG exhibited peaks at 2 $\theta$  of 7.9°, 8.8°, 23.1°, 23.9° and 24.4°, characteristic of diffraction peaks of ZSM-5. The characteristic peaks could not be obviously observed for the samples with dosage of PEG, indicating that the introduction of polyethylene glycol affected the crystallization of zeolite. The addition of polyethylene glycol coordinate with the metal ions, resulting in that Na<sup>+</sup>, was insufficient in the system, thereby making crystallization difficult.

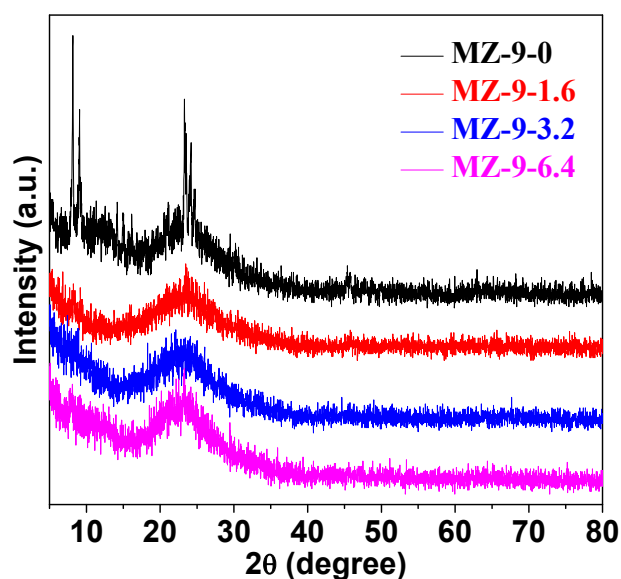


Figure 6. XRD patterns of MZ-9-0, MZ-9-1.6, MZ-9-3.2, and MZ-9-6.4.

The infrared spectra of samples with PEG dosage of 0, 1.6, 3.2, and 6.4 g are depicted in Figure 7. The Si-O-Si antisymmetric stretching vibration absorption peak was located at  $1228\text{ cm}^{-1}$ , the Si-O-Si symmetric stretching vibration peak was centered at  $800\text{ cm}^{-1}$ , and the five-membered ring characteristic absorption vibration peak due to the ZSM-5 zeolite structure was present at  $550\text{ cm}^{-1}$ , indicating that ZSM-5 or a molecular sieve containing ZSM-5 structural unit could be formed by this method. It is worth mentioning that the absorption peak at  $550\text{ cm}^{-1}$  of the sample without PEG was more obvious than the sample with PEG, indicating that the addition of PEG decreased the crystallization of ZSM-5, which is consistent with the XRD results.

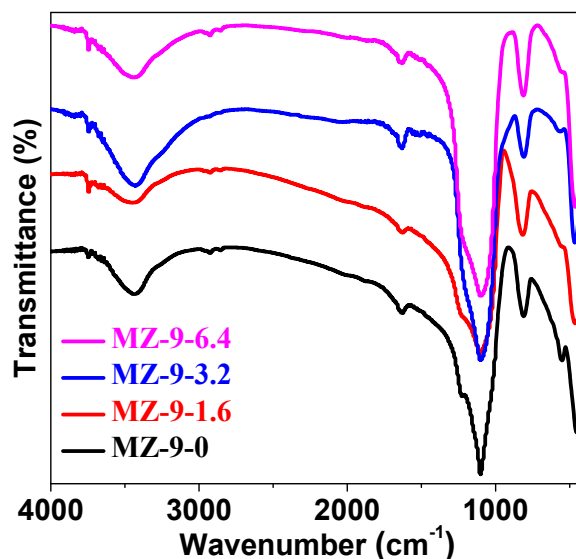
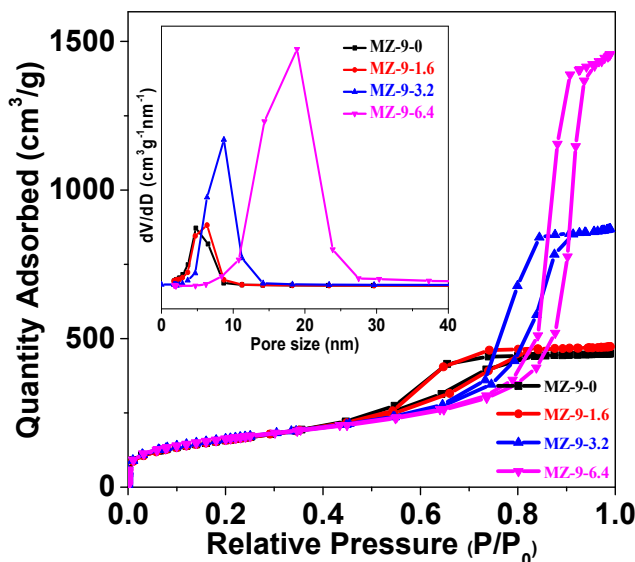


Figure 7. FT-IR spectra of MZ-9-0, MZ-9-1.6, MZ-9-3.2, and MZ-9-6.4.

The  $\text{N}_2$  adsorption–desorption isotherm curve and a BJH pore size distribution diagram of the synthetic samples with different PEG addition are depicted in Figure 8. The isotherm curve of the synthetic ZSM-5 sample without PEG addition was type IV, indicating the presence of mesoporous structure, which was attributed to the pile hole generated from the accumulation of small particles of ZSM-5. When the dosage of PEG was 1.6 g, the  $\text{N}_2$  adsorption–desorption isotherm curve of the

sample was a typical type IV adsorption isotherm curve, indicating that the addition of PEG formed a certain mesopore. When the dosage of PEG was increased to 3.2 g, the N<sub>2</sub> adsorption–desorption isothermal curve changed significantly. As the additional amount of PEG further increased, the N<sub>2</sub> adsorption–desorption isotherm curve of MZ-9-6.4 remained type IV, but the hysteresis loop was close to the H<sub>2</sub> type, indicating that the mesoporous structure was more regular.



**Figure 8.** N<sub>2</sub> adsorption–desorption isotherms and BJH pore size distributions of MZ-9-0, MZ-9-1.6, MZ-9-3.2, and MZ-9-6.4.

Table 4 shows the pore parameters of the samples. As the additional amount of PEG increased, the mesoporous size of the sample increased significantly. When the additional amount of PEG was 3.2 g, the specific surface area of the sample reached the highest. Since polyethylene glycol is a diol polymer with hydroxyl groups at both ends, a large amount of surface –OH causes steric hindrance when a large amount of PEG is added, this causes ions to become isolated from each other, leading to large species spacing during crystallization and increased pore size. The results of the N<sub>2</sub> adsorption–desorption isotherm curve, BJH pore size distribution, and pore parameters indicate that PEG is a good mesoporous soft template. By adding the appropriate amount of PEG, the mesoporous structure was introduced into ZSM-5 during crystallization, and a microporous–mesoporous material with a high specific surface area was obtained.

**Table 4.** Pore parameters of the samples.

Samples	$S_{\text{BET}}$ ( $\text{m}^2 \cdot \text{g}^{-1}$ )	Microporosity			Mesoporosity		
		Area ( $\text{m}^2 \cdot \text{g}^{-1}$ )	Size (nm)	Volume ( $\text{cm}^3 \cdot \text{g}^{-1}$ )	Area ( $\text{m}^2 \cdot \text{g}^{-1}$ )	Size (nm)	Volume ( $\text{cm}^3 \cdot \text{g}^{-1}$ )
MZ-9-0	570	40	–	0.01	530	4.8	0.68
MZ-9-1.6	573	34	–	0.01	539	6.3	0.72
MZ-9-3.2	581	75	–	0.03	506	11.3	1.34
MZ-9-6.4	581	75	–	0.03	506	18.9	2.21

The NH<sub>3</sub>-TPD spectra for samples of different amounts of PEG dosage are shown in Figure 9. The amount of added PEG has a large influence on the acidity of the sample. When the amount of PEG added was 0, 1.6 or 6.4 g, the curve was mainly dominated by the desorption peak of weak acid, indicating that the acid strength was weak. When the amount of added PEG is 3.2 g, two obvious NH<sub>3</sub>-desorption peaks appeared in MZ-9-3.2, corresponding to the desorption peaks of the weak acid and strong acid centers.



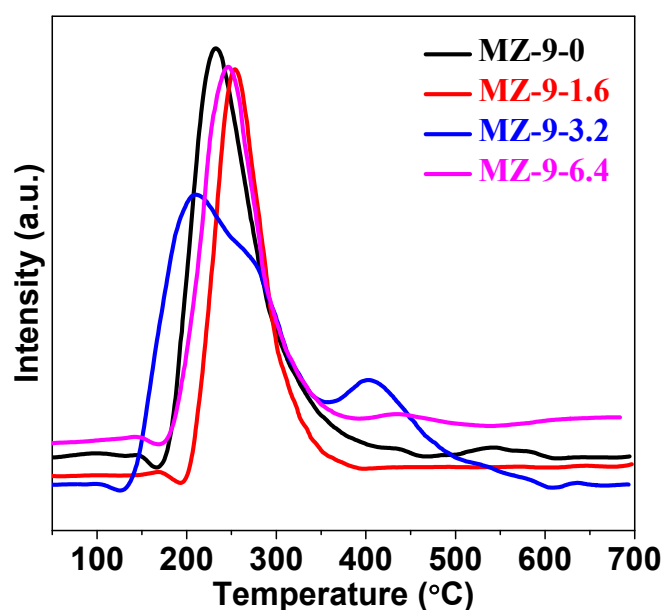


Figure 9.  $\text{NH}_3$ -TPD spectra of MZ-9-0, MZ-9-1.6, MZ-9-3.2, and MZ-9-6.4.

From Table 5, the catalytic performance of the sample with the addition of PEG has greatly improved, and the selectivity to 2,4-Di-tert-butylphenol is also increased. When the additional amount of PEG was 3.2 g, the highest conversion of phenol and highest selectivity to 2,4-Di-TBP were obtained, which was 96.5% and 53.9%, respectively. The addition of PEG to the synthesized ZSM-5 molecular sieve generates the mesoporous structure in the sample, which is beneficial to the catalytic reaction of phenol tert-butanol and the formation and transport of macromolecular products.

Table 5. The reaction results of the alkylation of phenol with tert-butanol. <sup>a</sup>

Catalysts	Conversion (%)	Selectivity (%)			
		2-TBP	4-TBP	2,4-Di-TBP	2,4,6-Tri-TBP
MZ-9-0	70.8	6.1	56.3	36.7	–
MZ-9-1.6	89.4	6.1	48.5	45.4	–
MZ-9-3.2	96.5	6.2	39.2	53.9	0.7
MZ-9-6.4	86.5	4.1	47.8	47.6	0.4

<sup>a</sup> Reaction conditions are the same as Table 2.

Hierarchically, porous molecular sieves are composed of two or more pore sizes, e.g., microporous and mesoporous coexistence. It combines the advantages of microporous and mesoporous channel structure, on which the catalytic application can be greatly extended. For example, the hierarchical pore catalysts can be applied in volatile organic compounds oxidation reaction [29]. In addition, the hierarchical porous molecular sieves have potential application in catalytic cracking reaction [30] and catalytic hydrogenation reaction [31], which makes the hierarchical porous materials important and useful in heterogeneous catalysis.

### 3. Experimental Section

#### 3.1. Main Reagents and Instruments

All reagents are analytical reagents. Sodium hydroxide (Beijing Chemical Plant), tetraethyl orthosilicate (Beijing Beihua Fine Chemicals Limited Company), aluminum sulfate (Xilong Chemical Plant, Shantou City, Guangdong Province), tetrapropylammonium hydroxide (Beijing Beihua Fine Chemicals Limited Company), ammonium nitrate (Beijing Chemical Plant), cetane trimethyl ammonium bromide

(Beijing Chemical Reagent Company), and polyethylene glycol (PEG, Wengjiang Chemical Plant, Guangdong Province) were used as received without further purification.

The following were also used: DF-101S aggregating heat constant temperature blender with magnetic force (Henan Province Yuhua Instrument Limited Company), DGX-9053BC-1 electric tachometer indicator thermostatic drying oven (Shanghai Fuma Experimental Equipment Limited Company), KBF1100 muffle furnace (Nanjing University Instrument Factory), Nicolet-5700 Fourier Infrared Spectrometer (Nikoli, USA), and Hitachi S4800 Transmission Electron Microscope (Japan Hitachi).

### 3.2. Catalyst Preparation

#### 3.2.1. Synthesis of Micro–Mesoporous ZSM-5 with Different Stirring Times

A total of 3.2 g of polyethylene glycol (PEG), 36 mL of water, 0.2 g of aluminum isopropoxide, and 10.36 g of tetraethyl orthosilicate were stirred at 40 °C for 30 min to obtain silica-alumina sol. Following this, 4.1 g of tetrapropylammonium hydroxide (TPAOH) was added to the above sol, which was stirred at exposure state for different times ( $t = 3, 6, 9,$  and  $15$  h) to form uniform transparent sol. The obtained sol was placed in a Teflon-lined reactor and crystallized at 150 °C. After 24 h the product was filtered, washed, dried and calcined in the air atmosphere at 550 °C for 5 h to remove the PEG and TPAOH template. The samples were named MZ-3-3.2, MZ-6-3.2, MZ-9-3.2, and MZ-15-3.2, respectively, according to the exposed stirring time.

#### 3.2.2. Synthesis of Micro–Mesoporous ZSM-5 with Different PEG Dosages

Different dosage of polyethylene glycol (0, 1.6, 3.2, and 6.4 g), 36 mL of water, 0.2 g of aluminum isopropoxide and 10.36 g tetraethyl orthosilicate were stirred at 40 °C for 30 min. Following this, 4.1 g of tetrapropylammonium hydroxide was added to the above sol and stirred for 9 h to form silica-alumina sol. The obtained sol was placed in a reactor and crystallized at 150 °C for 24 h. After which it was filtered, dried, and calcined in the air atmosphere at 550 °C for 5 h to remove the PEG and TPAOH template. The white powder was named MZ-9-0, MZ-9-1.6, MZ-9-3.2, MZ-9-6.4, respectively, according to the different PEG dosage. The Si:Al ratio of the obtained ZSM-5 was closed to 50:1 as detected by ICP-AES.

#### 3.2.3. Preparation of H-Type Micro–Mesoporous ZSM-5

A total of 1.5 g of micro–mesoporous ZSM-5 was added into ammonium nitrate solution and stirred for 5 h at 90 °C in a water bath to finish the first ion exchange. After being filtered and dried, the second ion exchange was carried out. The obtained ZSM-5 with twice ion exchange was placed in a muffle furnace and calcined at 500 °C for 5 h to obtain H-type micro–mesoporous ZSM-5.

#### 3.2.4. Catalytic Tests

Tert-butylation of phenol with tert-butanol was carried out in a fixed quartz bed reactor. H-type micro–mesoporous ZSM-5 at 0.5 g was used as a catalyst for the reaction. The alkylation reaction was investigated under reaction temperatures of 418 K. The  $n_{\text{tert-butanol}}/n_{\text{phenol}}$  ratio was 2.5. After the reaction was performed for 2 h, the products were collected and analyzed by a gas chromatograph. The area normalization method was used to obtain the conversion of phenol and the selectivity of each reaction product.

## 4. Conclusions

Due to its unique molecular structure, polyethylene glycol is suitable for the preparation of micro–mesoporous ZSM-5 as a mesoporous soft template. The micro–mesoporous ZSM-5 material synthesized by properly volatilizing the water solvent and adding a certain amount of PEG has a high overall surface area, a large pore size, and strong acidity, improving conversion of the reaction and

reducing diffusion resistance of the produced large molecule, thus showing higher catalytic activity and selectivity than the pure microporous ZSM-5.

**Author Contributions:** Writing-Original Draft Preparation, L.X.; Resources, F.W.; Resources, Z.F.; Project Administration, Z.L.; Writing-Review & Editing, J.G.

**Funding:** This work was financially supported by the National Natural Science Foundation of China (Grant No. 21561024 and 21661026).

**Conflicts of Interest:** The authors declare no conflict of interest.

## References

1. Kresge, C.T.; Leonowicz, M.E.; Roth, W.J.; Vartuli, J.C.; Beck, J.S. Ordered mesoporous molecular sieves synthesized by a liquid-crystal template mechanism. *Nature* **1992**, *359*, 710–712. [[CrossRef](#)]
2. Beck, J.S.; Vartuli, J.C.; Roth, W.J.; Leonowicz, M.E.; Kresge, C.T.; Schmitt, K.D.; Chu, C.T.W.; Olson, D.H.; Sheppard, E.W.; McCullen, S.B.; et al. A new family of mesoporous molecular sieves prepared with liquid crystal templates. *J. Am. Chem. Soc.* **1992**, *114*, 10834–10843. [[CrossRef](#)]
3. Zhao, D.Y.; Feng, J.L.; Huo, Q.S.; Melosh, N.; Fredrickson, G.H.; Chmelka, B.F.; Stucky, G.D. Triblock copolymer syntheses of mesoporous silica with periodic 50 to 300 angstrom pores. *Science* **1998**, *279*, 548–552. [[CrossRef](#)] [[PubMed](#)]
4. Zhao, D.Y.; Feng, J.L.; Huo, Q.S.; Chmelka, B.F.; Stucky, G.D. Nonionic triblock and star diblock copolymer and oligomeric surfactant syntheses of highly ordered, hydrothermally stable, mesoporous silica structures. *J. Am. Chem. Soc.* **1998**, *120*, 6024–6036. [[CrossRef](#)]
5. Janicke, M.T.; Landry, C.C.; Christiansen, S.C.; Birtalan, S.; Stucky, G.D.; Chmelka, B.F. Low Silica MCM-41 composites and mesoporous solids. *Chem. Mater.* **1999**, *11*, 1396–1397. [[CrossRef](#)]
6. Baute, D.; Zimmermann, H.; Kababya, S.; Vega, S.; Goldfarb, D. Synthesis of MCM-41 with a phosphonium template. *Chem. Mater.* **2005**, *17*, 3723–3727. [[CrossRef](#)]
7. Chiang, W.S.; Fratini, E.; Baglioni, P.; Georgi, D.; Chen, J.H.; Liu, Y. Methane adsorption in model mesoporous material, SBA-15, studied by small-angle neutron scattering. *J. Phys. Chem. C* **2016**, *120*, 4354–4363. [[CrossRef](#)]
8. Sayari, A.; Yang, Y. SBA-15 templated mesoporous carbon: new insights into the SBA-15 pore structure. *Chem. Mater.* **2005**, *17*, 6108–6113. [[CrossRef](#)]
9. Hoang, V.T.; Huang, Q.; Eić, M.; Do, T.O.; Kaliaguine, S. Structure and diffusion characterization of SBA-15 materials. *Langmuir* **2005**, *21*, 2051–2057. [[CrossRef](#)] [[PubMed](#)]
10. Linton, P.; Alfredsson, V. Growth and morphology of mesoporous SBA-15 particles. *Chem. Mater.* **2008**, *20*, 2878–2880. [[CrossRef](#)]
11. Yang, X.Y.; Chen, L.H.; Li, Y.; Rooke, J.C.; Sanchez, C.; Su, B.L. Hierarchically porous materials: Synthesis strategies and structure design. *Chem. Soc. Rev.* **2017**, *46*, 481–559. [[CrossRef](#)] [[PubMed](#)]
12. Petkov, N.; Hözl, M.; Metzger, T.H.; Mintova, S.; Bein, T. Ordered Micro/mesoporous composite prepared as thin films. *J. Phys. Chem. B* **2005**, *109*, 4485–4491. [[CrossRef](#)] [[PubMed](#)]
13. Huang, L.M.; Guo, W.P.; Deng, P.; Xue, Z.Y.; Li, Q.Z. Investigation of synthesizing MCM-41/ZSM-5 composites. *J. Phys. Chem. B* **2000**, *104*, 2817–2823. [[CrossRef](#)]
14. Jacobsen, C.J.H.; Madsen, C.; Houzvicka, J.; Schmidt, I.; Carlsson, A. Mesoporous zeolite single crystals. *J. Am. Chem. Soc.* **2000**, *122*, 7116–7117. [[CrossRef](#)]
15. Donk, S.; Janssen, A.; Bitter, J.; Jong, K.D. Generation, Characterization, and impact of mesopores in zeolite catalysts. *Catal. Rev.* **2003**, *45*, 297–319. [[CrossRef](#)]
16. Xiao, F.S.; Wang, L.; Yin, C.; Lin, K.; Di, Y.; Li, J.; Xu, R.; Su, D.S.; Schlögl, R.; Yokoi, T.; et al. Catalytic properties of hierarchical mesoporous zeolites templated with a mixture of small organic ammonium salts and mesoscale cationic polymers. *Angew. Chem. Int. Ed. Engl.* **2010**, *45*, 3090–3093. [[CrossRef](#)] [[PubMed](#)]
17. Tao, Y.; Kanoh, H.; Kaneko, K. ZSM-5 monolith of uniform mesoporous channels. *J. Am. Chem. Soc.* **2003**, *125*, 6044–6045. [[CrossRef](#)] [[PubMed](#)]
18. Serrano, D.P.; Aguado, J.; Escola, J.M.; And, J.M.R.; Peral, Á. Hierarchical zeolites with enhanced textural and catalytic properties synthesized from organofunctionalized seeds. *Chem. Mater.* **2006**, *18*, 2462–2464. [[CrossRef](#)]

19. Groen, J.C.; Jansen, J.C.; Moulijn, J.A.; Perez-Ramirez, J. Optimal aluminum-assisted mesoporosity development in MFI zeolites by desilication. *J. Phys. Chem. B* **2004**, *108*, 13062–13065. [[CrossRef](#)]
20. White, R.J.; Fischer, A.; Goebel, C.; Thomas, A. A sustainable template for mesoporous zeolite synthesis. *J. Am. Chem. Soc.* **2014**, *136*, 2715–2718. [[CrossRef](#)] [[PubMed](#)]
21. Guo, Y.P.; Wang, H.J.; Guo, Y.J.; Guo, L.H.; Chu, L.F.; Guo, C.X. Fabrication and characterization of hierarchical ZSM-5 zeolites by using organosilanes as additives. *Chem. Eng. J.* **2011**, *166*, 391–400. [[CrossRef](#)]
22. Liu, F.J.; Willhammar, T.; Wang, L.; Zhu, L.; Sun, Q.; Meng, X.; Carrillo-Cabrera, W.; Zou, X.; Xiao, F.S. ZSM-5 zeolite single crystals with b-axis-aligned mesoporous channels as an efficient catalyst for conversion of bulky organic molecules. *J. Am. Chem. Soc.* **2012**, *134*, 4557–4560. [[CrossRef](#)] [[PubMed](#)]
23. Anand, R.; Maheswari, R.; Gore, K.U.; Tope, B.B. Tertiary butylation of phenol over HY and dealuminated HY zeolites. *J. Mol. Catal. A Chem.* **2003**, *193*, 251–257. [[CrossRef](#)]
24. Huang, J.H.; Xing, L.H.; Wang, H.S.; Li, G.; Wu, S.J.; Wu, T.H.; Kan, Q.B. Tertiary butylation of phenol over hexagonal p6mm mesoporous aluminosilicates with enhanced acidity. *J. Mol. Catal. A Chem.* **2006**, *259*, 84–90. [[CrossRef](#)]
25. Zhang, K.; Zhang, H.B.; Xu, G.H.; Xiang, S.H.; Xu, D.; Liu, S.Y.; Li, H.X. Alkylation of phenol with tert-butyl alcohol catalyzed by large pore zeolites. *Appl. Catal. A Gen.* **2001**, *207*, 183–190. [[CrossRef](#)]
26. Sakthivel, A.; Badamali, S.K.; Selvam, P. Para-Selective t-butylation of phenol over mesoporous H-AlMCM-41. *Microporous Mesoporous Mater.* **2000**, *39*, 457–463. [[CrossRef](#)]
27. Terekhov, A.V.; Zhanaveskin, L.N.; Khadzhiev, S.N. Selecting an optimum catalyst for producing para-tert-butylphenol by phenol alkylation with tert-butanol. *Pet. Chem.* **2017**, *57*, 714–717. [[CrossRef](#)]
28. Chen, L.; Xue, T.; Wu, H.; Wu, P. Hierarchical ZSM-5 nanocrystal aggregates: Seed-induced green synthesis and its application in alkylation of phenol with tert-butanol. *RSC Adv.* **2018**, *8*, 2751–2758. [[CrossRef](#)]
29. Kamal, M.S.; Razzak, S.A.; Hossaina, M.M. Catalytic oxidation of volatile organic compounds (VOCs)—A review. *Atmos. Environ.* **2016**, *140*, 117–134. [[CrossRef](#)]
30. Louis, B.; Ocampo, F.; Yun, H.S.; Tessonier, J.P.; Pereira, M.M. Hierarchical pore ZSM-5 zeolite structures: From micro- to macro-engineering of structured catalysts. *Chem. Eng. J.* **2010**, *161*, 397–402. [[CrossRef](#)]
31. Ye, G.; Sun, Y.; Zhou, X.; Zhu, K.; Zhou, J.; Coppens, M.O. Method for generating pore networks in porous particles of arbitrary shape, and its application to catalytic hydrogenation of benzene. *Chem. Eng. J.* **2017**, *329*, 56–65. [[CrossRef](#)]

